crystals

MDPI

Article

The Use of Boron Fibers and Particles for Creating Functionally Graded Material Based on Ti64 Using the Laser Additive Manufacturing Method

Alexander Golyshev *, Alexander Malikov and Igor Vitoshkin

Khristianovich Institute of Theoretical and Applied Mechanics SB RAS, 4/1 Institutskaya Str., Novosibirsk 630090, Russia; smalik@ngs.ru (A.M.); igor.vitoshkin.97@mail.ru (I.V.)
* Correspondence: alexgol@itam.nsc.ru

Abstract: This work presents a study on the additive manufacturing of functionally graded metal-ceramic materials based on Ti64 with boron fibers and particles. For the first time, the phase composition of the obtained composite was investigated using synchrotron radiation. It was shown that during laser exposure and in situ synthesis, boron dissolves in the titanium matrix, forming secondary compounds such as TiB and TiB2. An increase in the microhardness of the formed material compared to the titanium alloy was established. High-speed impact tests on the Ti64-B samples were conducted using an electrodynamic mass accelerator. It was shown that the use of boron fibers in the metallic matrix reduces the depth of the crater created during impact testing by 40% compared to the Ti64 reinforcement-free coating.

Keywords: boron; high-speed impact; microstructure; crater formation; synchrotron radiation

check for updates

Citation: Golyshev, A.; Malikov, A.; Vitoshkin, I. The Use of Boron Fibers and Particles for Creating Functionally Graded Material Based on Ti64 Using the Laser Additive Manufacturing Method. *Crystals* **2023**, *13*, 1112. https://doi.org/10.3390/cryst13071112

Academic Editors: Damir Valiev and Sergey A. Stepanov

Received: 28 June 2023
Revised: 9 July 2023
Accepted: 12 July 2023
Published: 17 July 2023

Copyright: © 2023 by the authors. Licensee MDPI, Basel, Switzerland. This article is an open access article distributed under the terms and conditions of the Creative Commons Attribution (CC BY) license (https://creativecommons.org/licenses/by/4.0/).

1. Introduction

Currently, more than 70% of the global consumption of Ti and its alloys is accounted for in the aerospace industry [1]. This is due to their high-performance properties such as good resistance to corrosion and oxidation, high specific strength, and excellent damage resistance [2,3]. However, the main drawbacks of titanium alloys are their low wear resistance and hardness [4]. Thus, improving the physical and mechanical properties of titanium alloys can significantly expand their applications in various industries.

The addition of boron (B) to titanium alloys causes changes in the microstructure and an improvement in mechanical properties. It has been shown that adding a small amount of boron (up to 0.1% by weight) reduces the grain size of cast titanium alloys by an order of magnitude [5]. In addition, in situ synthesis occurs, resulting in the formation of secondary phase compounds such as TiB and TiB2 [6,7].

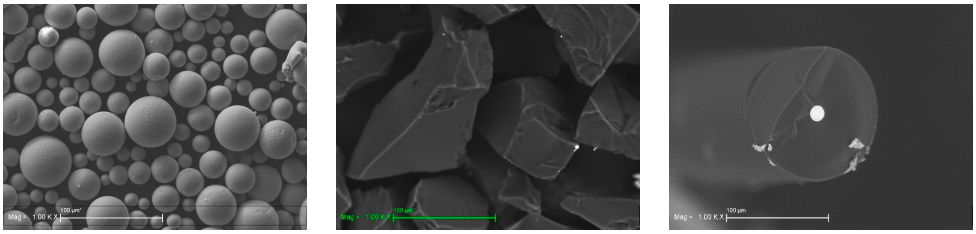
Titanium-matrix composites with intermittent reinforcement, TMCIR (ceramic particles or filamentary crystals), are considered one of the most promising structural materials [8]. However, compared to ex situ TMCIR, in situ ones have shown advantages such as strong bonding between the matrix and reinforcement and low pollution levels [9]. Nevertheless, the use of fibers instead of particles as reinforcing elements has not been investigated.

The application of TMCIR in the aerospace industry to provide effective protection against various external factors on the spacecraft body is a promising direction [10]. In [11,12], the impact of boron particle additives (up to 5 wt.%) in the titanium alloy Ti64 on the selective laser melting process was investigated. Significant changes in the microstructure and mechanical properties were observed compared to the titanium alloy. During the creation of the composites, a metallic matrix consisting of the Ti64 alloy and a ceramic phase TiB was formed. There have been no studies on the creation of metal–ceramic composites using boron fibers in additive manufacturing found in the literature.

The aim of this work was to determine the effect of the reinforcement shape on the resulting microstructure and impact-resistivity of a Ti/B composite. To achieve this goal, two types of coatings were produced: one with powder boron reinforcement and another with fiber boron as a reinforcement. The features of their microstructure were studied by SEM and X-ray diffraction (both with synchrotron and X-ray tube beam sources).

2. Materials and Methods

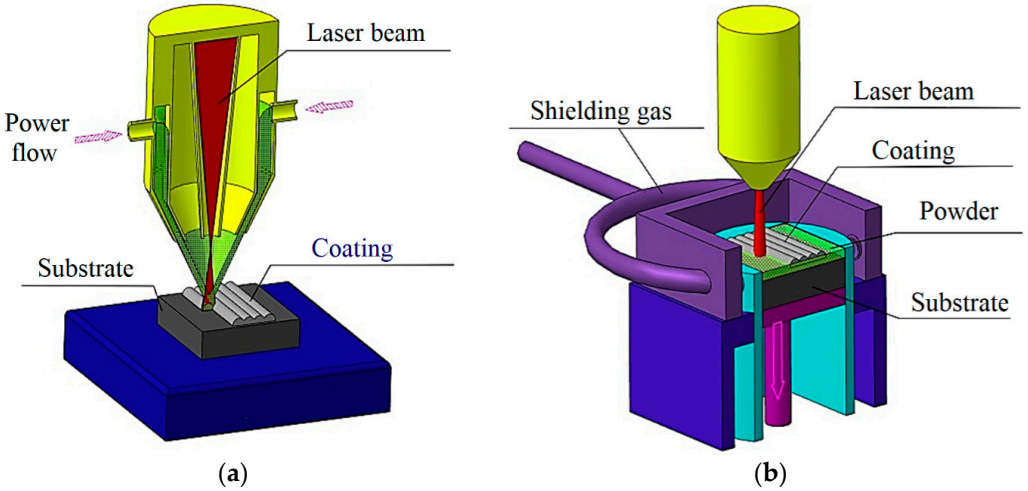
As a matrix material, a Ti64 alloy of sphere-shaped powder (10–45 μm) was applied in both cases (Figure 1a). For the powder reinforcement, a shard-shaped boron powder with sizes of 10–100 μm was used (Figure 1b). The role of fiber reinforcement was played by 100 μm thick boron fibers with tungsten core (Figure 1c). Both types of coatings were applied on similar Ti64 alloy substrates with sizes of 50 × 50 × 10 mm.



(**a**) (**b**) (**c**)

Figure 1. BSD images of the used powders: (**a**) Ti64, (**b**) boron particles, and (**c**) boron fiber.

For the creation of a metal–ceramic heterogeneous material using laser surface cladding (LSC) and direct metal deposition (DMD) methods, a ytterbium fiber laser from IPG Photonics with a wavelength of 1.07 μm and a maximum power of 3 kW was used. A schematic diagram of the laser technologies used is shown in Figure 2.



(**a**) (**b**)

Figure 2. Schematic diagram of the applied laser deposition methods: (**a**) direct laser deposition (DMD) technology and (**b**) laser surface cladding (LSC) technology.

A Ti64-B powder mixture with a 9:1 mass ratio was prepared by mixing the ingredients in a Venus FTLMV-02 V-mixer for one hour until a homogeneous powder mixture was formed. Then, the prepared powder mixture was applied to the DMD substrate (powder flow rate of 4 g/min, gas flow rate of 10 L/min).

To create a fiber-containing coating, the LSC method was used. Boron fibers were first ground in a self-designed high-energy planetary mill into a length of 300–600 μm. Crushed fibers were placed on the bottom layer of the substrate, and Ti64 powder was added on top as the second layer.

The Zeiss EVO MA 15 scanning electron microscope was used for microstructure evaluation in backscattered electron (BSE) mode. Experimental investigations of the durability of the created coatings were carried out using the high-speed interaction process of a striker and a target. The acceleration of the strikers was carried out using electromagnetic mass acceleration (EDUM) [13]. The principle of EDUM is based on the generation of an electromagnetic force acting on a current-carrying object located between the current-carrying channel walls (rails) when a current flows through the formed circuit. In this work, a plasma piston was used as the current-carrying object, exerting pressure on the accelerated container. A 0.5-g (diameter 4.8 mm) steel ball was used as the striker in this study. The interaction of the striker and the metal–ceramic coating was examined at a speed of 1150 m/s.

Since the composition of the surface layers of an impact-resistant material is critically important, it was studied separately with X-ray diffraction in addition to synchrotron radiation diffraction. To determine the phase composition, X-ray phase analysis was carried out on a D8 Advance X-ray diffractometer using the characteristic radiation of the copper anode of an X-ray tube Cu-Kα (λ = 1.5406 Å), a nickel filter to suppress the reflexion from Cu-Kβ radiation, and a linear position-sensitive detector, Lynx-Eye. Phase composition decoding was performed using the Springer Materials database.

To determine the phase composition throughout the volume of the material, synchrotron radiation (SR) research was carried out at the VEPP-3 located at the Budker Institute of Nuclear Physics, SB RAS, at the "diffraction in hard X-ray" station. A sample 1 mm thick was examined using SR radiation with a wavelength of 0.3685 Å in Debye–Sherrer geometry. The diameter of the beam was 100 μm. The sample-to-detector distance was 424 mm. Two-dimensional diffraction patterns were recorded with a Mar345 Image Plate Detector and the 2D patterns were transformed into 1D ones with an Area Diffraction Machine v1.0.5. Phase composition decoding was performed similarly to X-ray diffraction—with the Springer materials database.

3. Results

A search for energy parameters was conducted to obtain high-quality single tracks characterized by the absence of defects (pores and cracks). A search was also conducted to select the thickness of layers for the fiber coating, which resulted in selecting a layer thickness of 200 microns for crushed boron fiber and 400 microns for Ti64.

Table 1 shows the laser parameters and specific energy calculated as $J = 2W/(\pi \cdot r \cdot V)$ (W is the laser radiation power, V is the scanning speed, and r is the radius of the laser spot) used to obtain a functionally graded coating. In both cases, the coating thickness was approximately 3 mm.

Table 1. Optimal modes of laser exposure and energy conditions.

Sample	W, W	V, mm/s	d, mm	P, J/mm	J, J/mm^2
Ti64—B (particles)	1000	16	4.5	62.5	17.7
Ti64—V (fibers)	600	16	2.1	37.5	22.7

Figure 3 illustrates a metal-matrix multilayer material with boron particles and boron fibers at different magnifications obtained with an electron microscope.

In the coating with boron particles (Figure 3b), a more uniform distribution of reinforcing elements is observed compared to the sample with boron fiber (Figure 3a). In both cases, boron dissolves during interaction with the melt pool. According to literature data, boron reacts with the titanium alloy melt, leading to the formation of several titanium borides [14,15].

The diffraction pattern of the composite with fibers and boron particles is shown in Figure 4. As a result, secondary phase compounds such as TiB and TiB2 were detected in both samples.

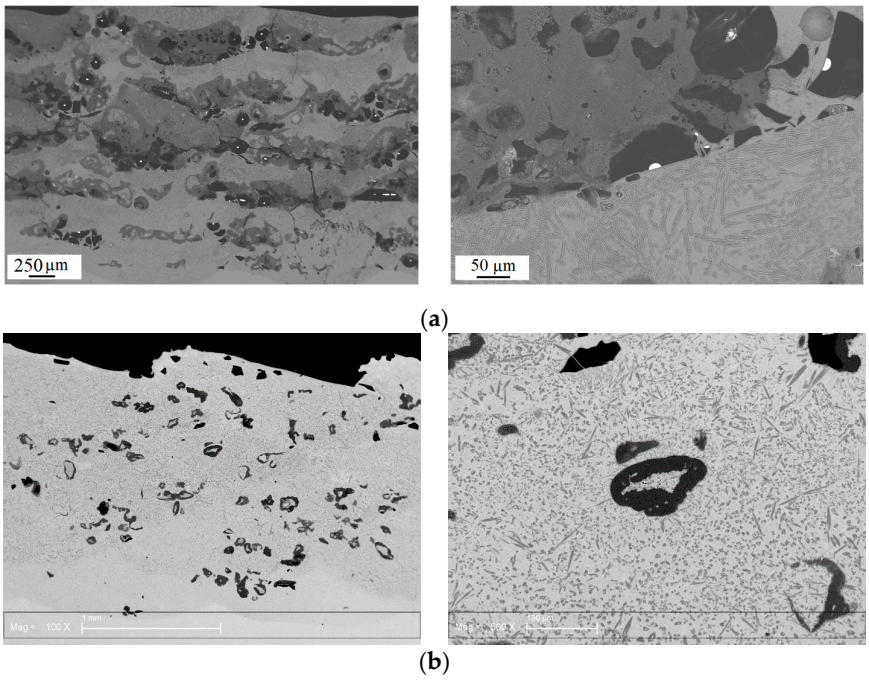


Figure 3. SEM image of a metal-matrix multilayer material ((**a**) Ti64 + boron fiber (LSC) and (**b**) Ti64 + boron powder (DMD)).

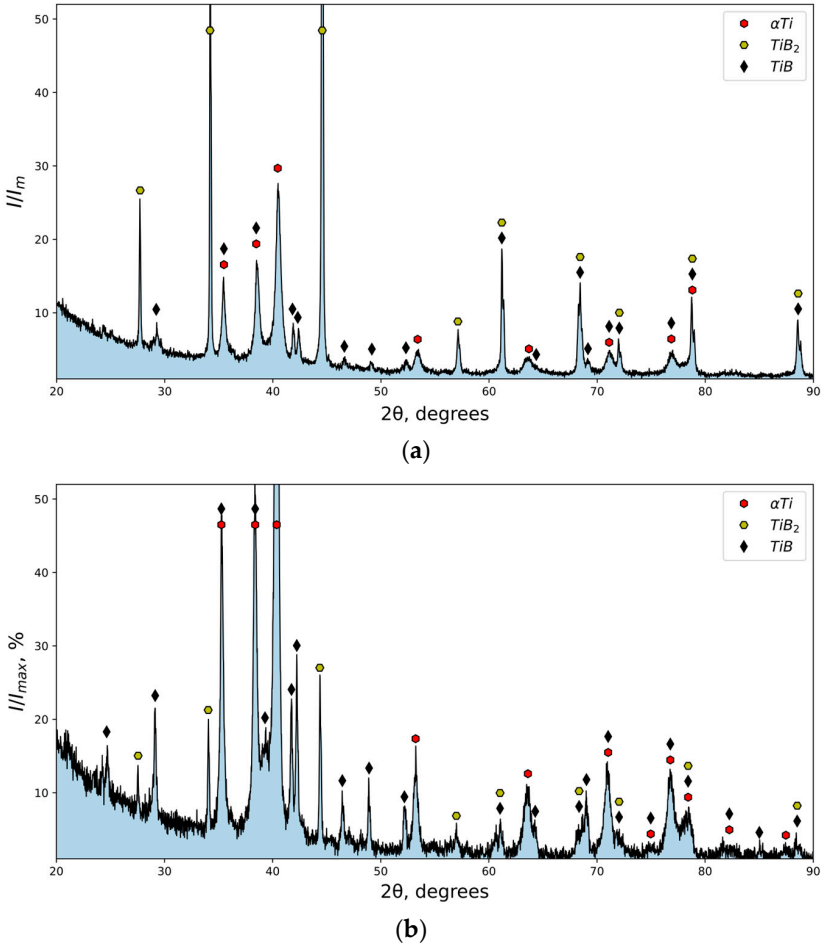


Figure 4. XRD pattern of Ti64 boron fiber (**a**) and Ti64 boron powder (**b**) specimens obtained using the diffractometer.

Table 2 presents the quantitative analysis results based on the XRD patterns shown in Figure 4. The XRD analysis of the coating surface revealed that titanium diboride (TiB2) formation was more active than titanium boride (TiB).

Table 2. Results of quantitative analysis (wt.%).

Phase Composition	αTi	TiB	TiB2
Ti64—B (particles)	0.7	0.22	0.08
Ti64—V (fibers)	0.29	0.1	0.61

However, data obtained by the RFA reflection method may not provide a complete picture of the information. It is important to understand what is happening inside the sample being studied. Synchrotron radiation was used for this purpose, which, due to its advantages, can penetrate a sample up to 2 mm thick.

From the diffraction patterns obtained using synchrotron radiation, diffraction diagrams were formed for samples of Ti64—boron powder and Ti64—boron fiber (Figure 5). Phase composition decoding was performed using the PDF4 database.

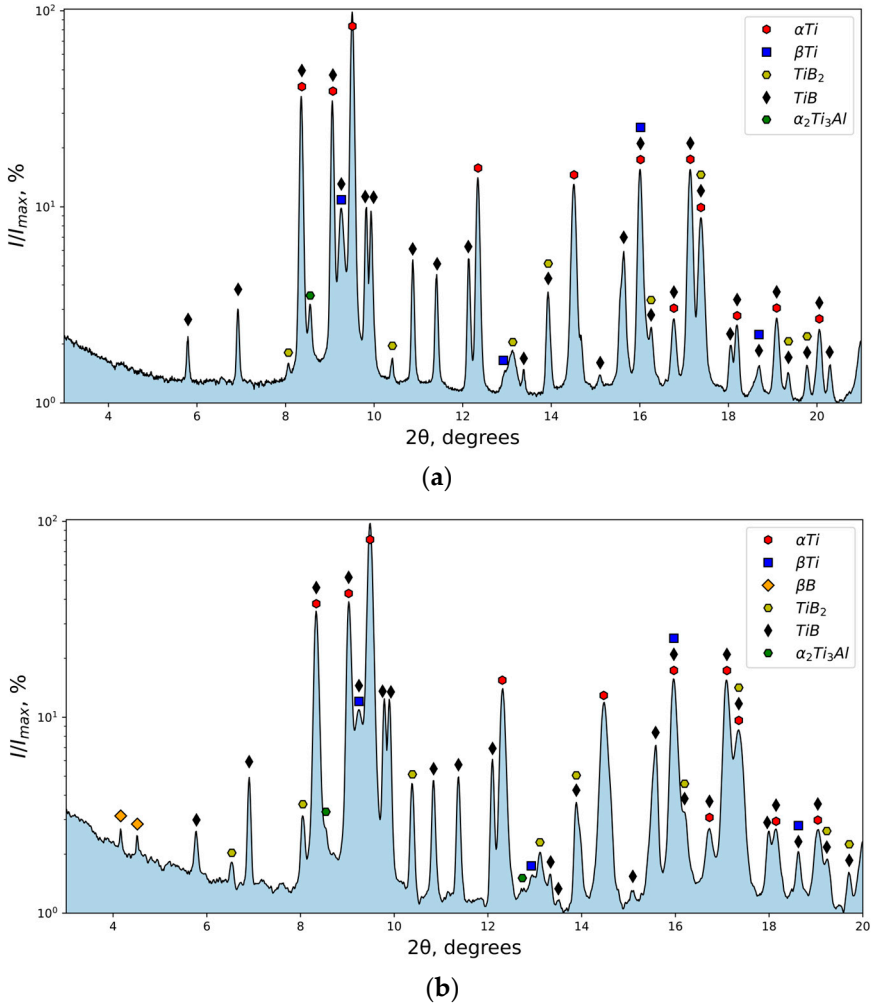


Figure 5. XRD for samples Ti64—boron fiber (**a**) and Ti64—boron powder (**b**).

The phase analysis (Figure 5) shows that the welding process with fiber led to the formation of titanium borides—TiB and TiB2. It can also be observed that a part of the original titanium alloy transformed into an ordered solid solution α2Ti3Al.

The coating shows a significant non-uniformity in the distribution of strengthening particles (see Figure 3). There are zones with extremely high concentrations of boron, where TiB2 is predominantly observed, as well as zones where few crystals of TiB2 are observed in the matrix of titanium and TiB mixture. Moreover, electron microscopy shows that boron fiber partially dissolved.

The more active filling of the metal matrix with secondary reinforcing compounds when using ceramic fiber indicates an increase in mechanical characteristics. Figure 6 shows the dependence of the microhardness of the metal–ceramic coating on the distance from the substrate (Figure 6). The microhardness values were averaged over three measurements for each distance. Indentation was performed in the matrix area without boron with a step of 200 μm between imprints.

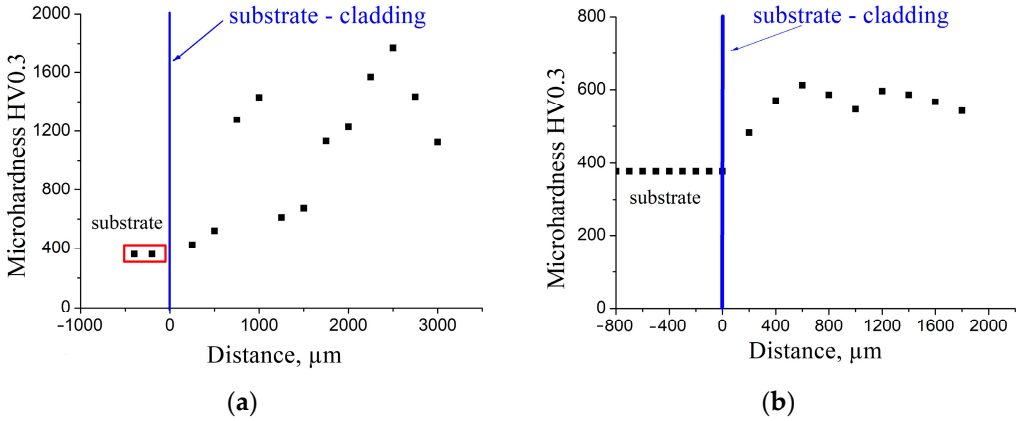


Figure 6. Microhardness distribution in the coatings: (**a**) with boron fibers and (**b**) with boron particles.

For samples with boron fiber, sharp drops in microhardness values are observed, indicating sample heterogeneity (Figure 6a). For samples with boron particles, a fundamentally different pattern is observed (Figure 6b). There is a gradual increase in microhardness to an approximate value of 600 HV0.3 which then remains constant due to secondary phase formations in this area (Figure 6b).

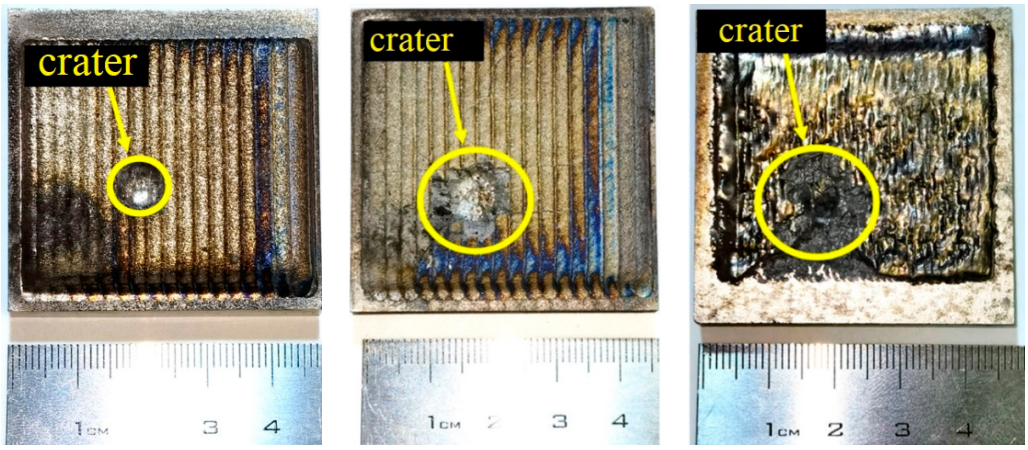
Due to the fact that the formed metal–ceramic composite materials represent a multilayer structure with significantly different morphology (see Figure 3), we can assume there are fundamentally different operational properties between the investigated samples.

Figure 7 shows the coatings after the impact tests. As a result of the interaction of the striker with the target, a crater with different types of destruction was formed.

It can be seen that during the high-speed interaction between the striker and the heterogeneous coating, the deposited layer was destroyed along the perimeter of the crater. Moreover, for the sample with boron fiber, the destruction occurs in the form of a disc (Figure 7c). For the sample with boron particles, the destruction occurs in the form of a hole with whitening (Figure 7b).

When studying the depth of the crater, it was found that for the Ti64 sample, the depth of the crater was 3.59 mm. In the case of using boron fiber, the depth of the crater decreased by 40% and amounted to 2.21 mm. The use of boron particles also allowed for a reduction in the depth of the crater to 2.59 (by 28% compared to Ti64), however, it showed worse results compared to the boron fiber.

The obtained results allow us to conclude that the coating with boron fibers provides effective dispersion of the kinetic energy of the striker throughout the sample volume, not just near the point of impact.



(**a**) (**b**) (**c**)

Figure 7. Photograph of the coating after impact resistance testing ((**a**) BT-6, (**b**) BT-6 powder B 9:1% by weight, and (**c**) BT-6 crushed boron fiber).

4. Discussion

Additive technologies are characterized by high heating and cooling rates, resulting in a locally concentrated high thermal gradient profile. According to [16], the effects caused by the temperature gradient must be combined with the main physical processes, such as mass and heat transfer, as well as the dynamics of the melt bath. Moreover, the gradient of surface tension caused by local temperature heterogeneity is considered the main driving force of Marangoni convection.

Microstructural changes resulting from melt crystallization depend on the temperature gradient parameter G and the crystallization rate R.

The solidification map of the melt bath was constructed using these parameters, as well as their combinations such as G·R and G/R. The G/R ratio determines the solidification mode, while G·R determines the size of the solidification microstructure [17]. The formation of the dendritic structure depends on the G/R ratio, and since laser deposition is characterized by a very high solidification rate, the melt bath has a structure consisting of dendritic grains. The connection between thermal impact, i.e., the cooling rate, and these parameters is represented by dT/dt = G·R.

In addition, dimensionless parameters allow for the determination of the processes taking place during additive technologies. For additive manufacturing, four groups of dimensionless variables are identified:

1. The Peclet number $Pe = \frac{Vb}{\alpha}$, where V is the scanning speed, b is the width of the melt bath, and α is the thermal conductivity of the alloy.
2. The dimensionless enthalpy $H = 2^{3/4} \cdot AW / \left(\rho C T_m \sqrt{\alpha V d^3}\right)$, where A is the integral absorption coefficient, ρ is the density of the material, C is the specific heat capacity, and d is the diameter of the laser spot.
3. The Marangoni number $a = -\frac{d\gamma}{dT}\frac{b\Delta T}{\mu\alpha}$, where μ is the viscosity of the alloy, ΔT is the difference between the peak temperature and the initial temperature of the alloy, and $\frac{d\gamma}{dT}$ represents the slope of the surface tension–temperature dependence curve.
4. The Fourier number $F = \frac{\alpha}{VL}$, where L is the characteristic length.

Together, these parameters can fully determine both the structure and characteristics of the materials formed by additive technologies [18,19].

There are important differences in the formation of the melt bath due to the difference in the energetic parameters between the two methods. When using boron particles, a functionally heterogeneous structure is observed, while fiber application results in a functionally heterogeneous and height gradient structure.

However, the specific energy levels (see Table 1) are similar for both cases, although the linear energy is different and related to the difference in powder deposition. The cooling rates are also similar, so it can be assumed that the in situ synthesis resulting from the interaction of titanium with boron plays a role in changing the structural and phase composition of the coatings. Additionally, the Marangoni number is an important parameter that includes the viscosity of the melt. Viscosity decreases with the addition of ceramic particles. However, the heat input is different, which may lead to changes in the melt bath width and thus affect the Peclet number, the ratio of specific energy absorbed by the material and the energy required for melting. This apparently determined the different structures of the arrays.

The interaction between metallic B and Ti has been studied in detail in various literature. According to the Ti–B phase diagram, the boron present dissolves in molten titanium [20,21].

Diffraction data analysis results have shown that both boron powder and boron fibers dissolve in a titanium matrix to form secondary compounds such as TiB and TiB2, which were not originally present in the mixture. These new compounds were synthesized through a chemical reaction between the elements within the metallic matrix. In our case, the laser treatment of the Ti64 + B mixture resulted in the formation of TiB2 ceramics, while the in situ synthesis of TiB2 ceramics interacted with titanium to form TiB ceramics. This was confirmed by XRD, which shows a higher concentration of TiB2 ceramics in the titanium matrix than TiB.

Phase analysis revealed (Figure 5) that the cladding process resulted in the formation of titanium borides—TiB and TiB2. It is also observed that a portion of the original titanium alloy underwent a transformation into an ordered solid solution α2Ti3Al.

The resulting coating had a significant non-uniformity of reinforcing particle distribution. There were zones with an extremely high boron concentration that mainly showed TiB2, and zones with few TiB2 crystals in a matrix of a titanium and TiB mixture. Electron microscopy revealed that the boron fiber had only partially dissolved.

In boron-rich areas, the TiB2 particles were chemically heterogeneous, with a layer enriched with heavy elements visible on their surface (see Figure 8). Table 3 presents the results of the spectral analysis of Figure 8a. As the T–B system exhibits a peritectic reaction, L + TiB2 → Ti3B4, it is possible to assume that this reaction may have been initiated but not fully completed, as it occurs in a very narrow (~20 K) temperature range [22]. This assumption is supported by the fact that the products of this reaction are located on the surface of TiB2. However, as shown, Ti3B4 was not detected during phase analysis (Figure 5).

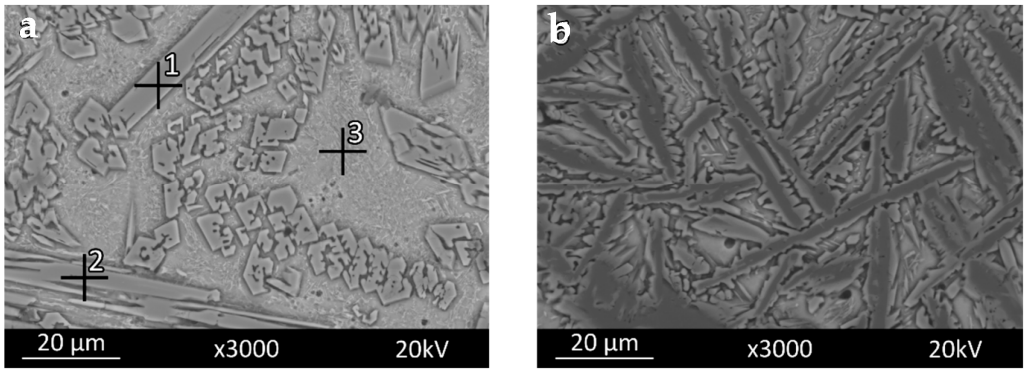


Figure 8. Microstructure of layers with a low (**a**) and high (**b**) boron content for sample Ti64-boron fiber.

Table 3. Results of the spectral analysis of Figure 8a.

Point	Ti, at.%	B, at.%	Al, at.%	V, at.%
1	35.86	62.98	-	1.16
2	36.65	62.11	-	1.24
3	54.11	39.73	4.26	1.89

The significant dissolution of boron leads to the binding of titanium, and the concentration of aluminum in the titanium solid solution was sufficient for its ordering and transformation into α2Ti3Al. As the phase analysis of the boron fiber coating showed the presence of both a disordered (α and β) and ordered solid solution (α2), it can be assumed that in areas with a high boron content of titanium, enough was bound for ordering in the residue of the metallic matrix, while in other areas the disordered solid solution remained. In this case, ordering in the already richly fragile phase region will lead to additional strengthening and at the same time to embrittlement.

In contrast to the results obtained using X-ray diffraction on reflection, the use of synchrotron radiation allowed for the determination of βTi in both cases, and, for the sample with boron powder, an additional intermetallic phase α2 Ti3Al was synthesized.

In this case, TiB2 probably played the role of a β stabilizer according to the Ti–B diagram, which allowed the formation of α and β-Ti in the obtained TMC. When the laser touched the B-Ti64 powder mixture, melting occurred with a transition to a liquid phase.

Increasing the boron concentration in the starting mixture will lead to an increase in the viscosity of the melt and a decrease in the Marangoni convection.

At the same time, compared to Ti, B has a higher laser absorption rate [23,24], which improves the laser-absorbing ability of B–Ti powders. Increasing the boron content in the starting mixture allowed us to increase the absorption coefficient, thus increasing the absorbed energy and temperature in the melt baths and changing the enthalpy. There was strong mixing, which made it possible to actively carry out the reaction Ti + TiB2 → 2TiB, with the formation of mainly TiB. Apparently, TiB2 dissolved in liquid titanium. If the liquid had a sub-eutectic composition, titanium crystallized first, after which the eutectic crystallized. If the liquid was obtained hypo-eutectic, primary TiB crystallized first, after which the eutectic crystallized.

However, B did not react fully with titanium. Electron microscopy and X-ray phase analysis confirm the presence of boron. Boron did not have enough time to dissolve and remained suspended in the molten bath until its crystallization. These effects are apparently related to the imbalance in the crystallization process due to laser radiation and the reduction in the Marangoni number. The driving force energy is different for the two methods, which can lead to differences in the width of the molten bath and changes in the Marangoni, Peclet, and dimensionless enthalpy.

Accordingly, the development of a functionally heterogeneous and height-gradient structure is influenced by the in situ synthesis resulting from the interaction of titanium with boron, the imbalance of the crystallization processes due to laser irradiation, the laser absorption coefficient, the change in melt convection, specific energy absorbed by the material, and energy required for melting by convective and conductive heat transfer. The developed structure allows for the fundamentally different operational properties of the investigated samples depending on the created coating. For the sample with boron fiber, the destruction after an impact occurs in the form of a disc, and for the sample with boron particles, the destruction occurs in the form of a hole with a rim. At the same time, the microhardness of the functionally heterogeneous gradient coating with boron fiber is higher than the functionally heterogeneous coating with fiber particles.

5. Conclusions

A metal–ceramic heterogeneous material, with a titanium matrix reinforced with boron fibers and particles, was formed using the additive growth method. The stages of damage

(crater formation) and transition to destruction of the formed material were studied during a high-speed impact using an electrodynamic mass accelerator.

The phase composition of the obtained composite was investigated using synchrotron radiation at the "MegaScience" facility (Institute of Nuclear Physics, SB RAS). It was shown that, as a result of laser treatment, boron dissolves in the titanium matrix, forming secondary compounds such as TiB and TiB2.

It has been established that the use of boron particles results in a functionally heterogeneous structure, while the use of fibers leads to a functionally heterogeneous and height-gradient structure.

The structural and phase composition is mainly determined by the in situ synthesis resulting from the interaction of titanium with boron, the non-equilibrium course of crystallization processes under laser irradiation, and changes in the Marangoni convection.

It has been shown that the use of boron fibers in a metal matrix results in a 40% reduction in impact crater depth compared to particles with a Ti64 coating.

The provided work makes it clear how the shape of the reinforcement influences the impact resistivity of the composite. Further study will be devoted to the effect of the boron fiber length on the properties and microstructure of the Ti/B composites.

Author Contributions: Conceptualization, A.M. and A.G.; methodology, A.M.; investigation, A.M., I.V., and A.G.; data curation, A.G.; writing—original draft preparation, A.G.; writing—review and editing, A.M., I.V., and A.G.; supervision, A.G.; project administration, A.G.; funding acquisition, A.G. All authors have read and agreed to the published version of the manuscript.

Funding: This research was funded by Russian Scientific Foundation, grant number 21-79-10213 (https://rscf.ru/project/21-79-10213/). Part of the work was performed at the shared research center SSTRC on the basis of the VEPP-4—VEPP-2000 complex at BINP SB RAS.

Informed Consent Statement: Informed consent was obtained from all subjects involved in the study.

Data Availability Statement: Not applicable.

Acknowledgments: Thanks to the research associates of Laboratory №4 of the Institute of Theoretical and Applied Mechanics of the Siberian Branch of the Russian Academy of Sciences, Filippov A.A. and Yadrenkin M.A.

Conflicts of Interest: The authors declare no conflict of interest.

References

1. Cui, C.; Hu, B.; Zhao, L.; Liu, S. Titanium alloy production technology, market prospects and industry development. *Mater. Des.* **2011**, *32*, 1684–1691. [CrossRef]
2. Boyer, R.R. An overview on the use of titanium in the aerospace industry. *Mater. Sci. Eng. A* **1996**, *213*, 103–114. [CrossRef]
3. Gorynin, I.V. Titanium alloys for marine application. *Mater. Sci. Eng. A* **1999**, *263*, 112–116. [CrossRef]
4. Golyshev, A.; Malikov, A.; Orishich, A.; Gulov, M.; Ancharov, A. The effect of using repetitively pulsed laser radiation in selective laser melting when creating a metal-matrix composite Ti-6Al-4V–B4C. *Int. J. Adv. Manuf. Technol.* **2021**, *117*, 1891–1904. [CrossRef]
5. Singh, G.; Ramamurty, U. Reprint: Boron modified titanium alloys. *Prog. Mater. Sci.* **2021**, *120*, 100815. [CrossRef]
6. Lu, W.; Zhang, D.; Zhang, X.; Wu, R.; Sakata, T.; Mori, H. Creep rupture life of in situ synthesized (TiB + TiC)/Ti matrix composites. *Scr. Mater.* **2001**, *44*, 2449–2455. [CrossRef]
7. Morsi, K.; Patel, V.V. Processing and properties of titanium–titanium boride (TiBw) matrix composites—A review. *J. Mater. Sci.* **2007**, *42*, 2037–2047. [CrossRef]
8. Li, S.; Wang, X.; Le, J.; Han, Y.; Zong, N.; Wei, Z.; Huang, G.; Lu, W. Towards high strengthening efficiency by in-situ planting nano-TiB networks into titanium matrix composites. *Compos. B Eng.* **2022**, *245*, 110169. [CrossRef]
9. Tjong, S.C.; Mai, Y.-W. Processing-structure-property aspects of particulate- and whisker-reinforced titanium matrix composites. *Compos. Sci. Technol.* **2008**, *68*, 583–601. [CrossRef]
10. Kraus, A.; Buzyurkin, A.; Shabalin, I.; Kraus, E. Numerical Modelling of High-Speed Loading of Periodic Interpenetrating Heterogeneous Media with Adapted Mesostructure. *Appl. Sci.* **2023**, *13*, 7187. [CrossRef]
11. Verma, P.K.; Warghane, S.; Nichul, U.; Kumar, P.; Dhole, A.; Hiwarkar, V. Effect of boron addition on microstructure, hardness and wear performance of Ti-6Al-4 V alloy manufactured by laser powder bed fusion additive manufacturing. *Mater. Charact.* **2021**, *172*, 110848. [CrossRef]
12. He, Y.; Montgomery, C.; Beuth, J.; Webler, B. Melt pool geometry and microstructure of Ti6Al4V with B additions processed by selective laser melting additive manufacturing. *Mater. Des.* **2019**, *183*, 108126. [CrossRef]

13. Fomin, V.M.; Golyshev, A.A.; Malikov, A.G.; Filippov, A.A.; Shikalov, V.S.; Yadrenkin, M.A.; Orishich, A.M. Experimental Investigation of the Effect of Laser Treatment on the Resistance of a Cermet Coating to a High-Speed Impact. *J. Eng. Phys. Thermophys.* **2022**, *95*, 1773–1779. [CrossRef]
14. Krakhmalev, P.; Yadroitsev, I. Microstructure and properties of intermetallic composite coatings fabricated by selective laser melting of Ti-SiC powder mixtures. *Intermetallics* **2014**, *46*, 147–155. [CrossRef]
15. Polozov, I.; Sufiiarov, V.; Starikov, K.; Popovich, A. In situ synthesized Ti2AlNb-based composites produced by selective laser melting by addition of SiC-whiskers. *Mater. Lett.* **2021**, *297*, 129956. [CrossRef]
16. Yang, Y.; Kühn, P.; Yi, M.; Egger, H.; Xu, B.X. Non-isothermal Phase-Field Modeling of Heat–Melt–Microstructure-Coupled Processes During Powder Bed Fusion. *JOM* **2020**, *72*, 1719–1733. [CrossRef]
17. Kurz, W.; Giovanola, B.; Trivedi, R. Theory of microstructural development during rapid solidification. *Acta Metall.* **1986**, *34*, 823–830. [CrossRef]
18. Yang, Y.; Großmann, A.; Kühn, P.; Mölleney, J.; Kropholler, L.; Mittelstedt, C.; Xu, B.X. Validated dimensionless scaling law for melt pool width in laser powder bed fusion. *J. Mater. Process. Technol.* **2022**, *299*, 117316. [CrossRef]
19. Mukherjee, T.; Manvatkar, V.; De, A.; DebRoy, T. Dimensionless numbers in additive manufacturing. *J. Appl. Phys.* **2017**, *121*, 064904. [CrossRef]
20. Murray, J.L.; Liao, P.K.; Spear, K.E. The B−Ti (Boron-Titanium) system. *Bull. Alloy Phase Diagr.* **1986**, *7*, 550–555. [CrossRef]
21. Fomin, V.M.; Golyshev, A.A.; Malikov, A.G.; Orishich, A.M.; Filippov, A.A. Creation of a Heterogeneous Material Based on the Titanium Alloy and Titanium Boride by Selective Laser Melting. *J. Appl. Mech. Tech. Phys.* **2020**, *61*, 878–887. [CrossRef]
22. De Graef, M.; Löfvander, J.P.A.; McCullough, C.; Levi, C.G. The evolution of metastable Bf borides in a Ti-Al-B alloy. *Acta Metall. Mater.* **1992**, *40*, 3395–3406. [CrossRef]
23. Chen, C.; Gu, D.; Dai, D.; Du, L.; Wang, R.; Ma, C.; Xia, M. Laser additive manufacturing of layered TiB2/Ti6Al4V multi-material parts: Understanding thermal behavior evolution. *Opt. Laser Technol.* **2019**, *119*, 105666. [CrossRef]
24. Wang, R.; Gu, D.; Chen, C.; Dai, D.; Ma, C.; Zhang, H. Formation mechanisms of TiB2 tracks on Ti6Al4V alloy during selective laser melting of ceramic-metal multi-material. *Powder Technol.* **2020**, *367*, 597–607. [CrossRef]

Disclaimer/Publisher's Note: The statements, opinions and data contained in all publications are solely those of the individual author(s) and contributor(s) and not of MDPI and/or the editor(s). MDPI and/or the editor(s) disclaim responsibility for any injury to people or property resulting from any ideas, methods, instructions or products referred to in the content.